Microchimica Acta (2020) 187: 264
https://doi.org/10.1007/s00604-020-04235-5

ORIGINAL PAPER

Electrochemical immunoassay for the carcinoembryonic antigen based on Au NPs modified zeolitic imidazolate framework and ordered mesoporous carbon

Yingcong Zhang[1] · Ze Zhang[1] · Shengzhong Rong[1,2] · Hongwei Yu[1] · Hongmin Gao[3] · Ping Ding[4] · Dong Chang[1] · Hongzhi Pan[5]

Received: 1 November 2019 / Accepted: 24 March 2020 / Published online: 8 April 2020

Abstract

An electrochemical immunoassay for the carcinoembryonic antigen is described. It is based on the use of Au NPs modified zeolitic imidazolate framework (ZIF-8) and ordered mesoporous carbon (OMC). Au NPs@ZIF-8 was synthesized by reduction of chloroauric acid. It serves as immobilization support nanocarrier to increase antibody loading due to its large surface area. OMC was dropped on a glassy carbon electrode to improve electrochemical signals due to enhanced electrical conductivity. Differential pulse voltammetry was carried out to record electrochemical responses (best measured at 0.26 V vs. Ag/AgCl). The immunosensor demonstrated excellent electrochemical performance with a linear determination range of 5 pg mL^{-1} to 400 ng mL^{-1} and a determination limit of 1.3 pg mL^{-1} ($S/N = 3$). The sensor also exhibited high selectivity, good stability, and acceptable reproducibility.

Keywords CEA · Immunosensor · ZIF-8 · Gold nanoparticles

Introduction

Carcinoembryonic antigen (CEA) is a tumor marker normally expressed in limited areas of human body. Overexpression of CEA contributes to improving the diagnosis of many diseases, including colorectal cancer [1], lung cancer [2], breast cancer [3], pancreatic cancer [4], and many other benign tumors [5]. Various immunological methods have been exploited for CEA determination, including electrochemical immunoassay [6, 7], photoelectrochemical immunoassay [8], fluoroimmunoassay [9], chemiluminescence immunoassay [10, 11], plasmonic immunosensor [12], and so on.

Electrochemical immunoassay is identified as the predominant analytical determination technology for clinical diagnosis due to its advantages such as cost effectiveness, extremely high sensitivity, fast response, and easy operation [13, 14]. Since an immunosensor is constructed based on high affinity of antigen and antibody, it is extremely important to increase antibody immobilization on the electrochemical platform surface. Hence, searching for a reliable and suitable material for effective antibody immobilization is still a crucial subject to explore.

Zeolitic imidazolate frameworks-8 (ZIF-8) as a representative of metal-organic framework (MOF) has a typical sodalite

Yingcong Zhang and Ze Zhang contributed equally to this work.

Electronic supplementary material The online version of this article (https://doi.org/10.1007/s00604-020-04235-5) contains supplementary material, which is available to authorized users.

✉ Dong Chang
changdongydy@163.com

✉ Hongzhi Pan
panhongzhi@163.com

[1] Department of Clinical Laboratory, Shanghai Pudong Hospital, Fudan University, Shanghai 200000, People's Republic of China

[2] Public Health School, Mudanjiang Medical University, Mudanjiang 157011, Heilongjiang, People's Republic of China

[3] School of Public Health, Wuhan University of Science and Technology, Wuhan, HuBei Province 430065, People's Republic of China

[4] Xiang Ya School of Public Health, Central South University, Changsha 410078, People's Republic of China

[5] Collaborative Research Center, Shanghai University of Medicine and Health Sciences, Shanghai 201399, People's Republic of China

structure and a large specific surface area. Compared with other MOF materials, ZIF-8 has many advantages such as exceptional hydrothermal and chemical stability, a large pore volume, and a uniform pore structure [15–17]. These advantages enable ZIF-8 to provide a promising sensing layer for increasing antibody loading. In particular, an ultra-high surface area is one of the most important advantages of ZIF-8. This advantage makes ZIF-8 have considerable potential in serving as immobilization support nanocarriers in biomedical applications. For example, Dong et al. successfully synthesized heterogeneous composite ZnO@ ZIF-8 nanorods, using ZnO@ZIF-8/IL composite film as an immobilization matrix to construct an immunosensor for the determination of human IgG [18]. Wang et al. used zeolitic imidazolate framework-hydroquinone-bovine serum albumin (ZIF-8-HQ-BSA) as immunosensor probes to detect cytokeratin antigen 21-1 [19].

Ordered mesoporous carbon (OMC), a new type of carbon nanomaterials with ordered pores, has been applied widely in sensors due to its excellent properties such as high specific surface area, high thermal stability, flexible structure, electrical conductivity, and good biocompatibility [20–22]. OMC with excellent properties is especially desirable for efficient immobilization of nanomaterials and biomolecules. For example, Yang et al. used Au@CMK-3 nanocomposite as nanocarriers for highly dense immobilization of methylene blue and secondary antibodies for determination of prostate-specific antigen [23]. In addition, OMC is intrinsically a good conductor and exhibits outstanding advantages in electrical conductivity. The uniform and ordered porous structure of OMC provides a more advantageous route for electrolyte penetration and transportation.

In this work, an electrochemical immunosensor was constructed for CEA determination based on Au NPs modified ZIF-8 and ordered mesoporous carbon. Au NPs modified ZIF-8 nanoparticles (Au@ZIF-8) was successfully synthesized by reduction of $HAuCl_4$ to improve antibody loading. Antibodies were immobilized on the surface of Au@ZIF-8 via Au-N bonds. Ordered mesoporous carbon with high specific surface area and good electrical conductivity was dropped on the surface of electrode to provide support matrix for Au@ZIF-8 and enhance the conductivity of an immunosensor. Electrochemical properties of biosensors were enhanced by the synergistic effect among Au NPs, ZIF-8, and OMC. The immunosensor shows a wide linear determination range with a low determination limit; therefore, it has extensive application perspective for CEA determination.

Materials and methods

Materials

CEA, anti-CEA antibodies, and alpha fetoprotein (AFP) were purchased from Abcam Co., England (www.abcam.com/). $Zn(NO3)_2{\cdot}6H_2O$, methanol, immunoglobulin G (IgG), and human chorionic gonadotropin (HCG) were brought from Sigma-Aldrich Chemicals Co., USA (www.sigmaaldrich.com/). 2-Methylimidazole, chloroauric acid, potassium ferricyanide ($K_3Fe(CN)_6$), and potassium ferrocyanide ($K_4Fe(CN)_6$) were bought from Adamas Reagent Co., Ltd., China (www.adamas-beta.com/). OMC was purchased from Nanjing JCNANO Tech Co., Ltd., China (www.jcno.net/). Potassium chloride (KCl) was purchased from Shanghai Titan Scientific Co., Ltd., China (www.titansci.com/). Bovine serum albumin (BSA) was purchased from Yeasen Biotech Co., Ltd., China (www.yeasen.com/). All reagents used were of analytical grade and used without further purification. Deionized water was used for all experiments. The serum samples were provided by Shanghai Pudong Hospital. CEA and anti-CEA antibodies were dissolved with 0.01 mol L^{-1} phosphate buffer saline (PBS).

Apparatus

Transmission electron microscope (TEM) images were collected on a JEOL JEM-2100F field emission TEM. Scanning electron microscope (SEM) images were acquired using a Hitachi S-4800 field-emission SEM. The Fourier transform infrared spectroscopy spectra were collected on a PerkinElmer Spectrum 100 Fourier transform infrared spectrometer (FTIR). Raman spectroscopy spectra were measured with a Renishaw inVia Reflex Raman spectrometer. X-Ray diffraction (XRD) patterns were measured with a Rigaku D/max-2600PC X-ray diffractometer. X-Ray photoelectron spectroscopy (XPS) images were recorded with a Thermo Fisher ESCALAB 250Xi X-ray photoelectron spectrometer.

Electrochemical measurements

Electrochemical experiments were performed with a CHI660E electrochemical workstation (Chenhua Instrument Shanghai Co., Ltd., China, www. chinstr.com) with a conventional three-electrode system. The modified glassy carbon electrode (GCE, 3 mm in diameter) acted as the working electrode. Glassy carbon electrode can be reused with high repeatability by a simple grinding treatment after measurement. A saturated calomel electrode (SCE) was used as the reference electrode while a platinum plate served as the auxiliary electrode. Cyclic voltammetry (CV) was performed at a scan rate of 50 mV s^{-1}. Electrochemical impedance spectroscopy (EIS) was measured from 100 kHz to 1 Hz with signal amplitude of 5 mV. Differential pulse voltammetry was performed from 0 to 0.6 V with a pulse amplitude of 50 mV and width of 50 ms. Electrochemical experiments were carried out in 0.1 M phosphate buffer that contained 5 mM $Fe(CN)_6^{3-/4-}$ and 0.1 M KCl.

Synthesis of ZIF-8

ZIF-8 was synthesized using procedures previously reported in the literature [24]. Forty milliliters of $Zn(NO3)_2 \cdot 6H_2O$ methanol solution (0.1 mol L^{-1}) was quickly poured into 40 mL 2-methylimidazole methanol solution (0.1 mol L^{-1}) and stirred for 1 h. Milky white solution was collected, centrifuged, and repeatedly washed with methanol for several times to collect white precipitate. The white precipitate was dried in a vacuum oven under 50 °C to collect ZIF-8 powder.

Synthesis of Au@ZIF-8 nanoparticles

One hundred milligrams of ZIF-8 powder was dispersed in methanol solution with ultrasonication for 30 min. A total of 426 μL chloroauric acid methanol solution (0.1 g mL^{-1}) was added into the uniformly dispersed ZIF-8 methanol solution. A total of 2.5 mL $NaBH_4$ methanol solution (0.01 M) was then added into the above mixture and stirred vigorously. The solution gradually turns purple under stirring. After 1 h, the mixture was centrifuged to collect a light purple precipitate. The resulting precipitate was separated from the solution and washed several times with methanol, and dried in a vacuum oven under 50 °C to collect Au@ZIF-8 nanoparticles.

Fabrication of immunosensor

Before modification, GCE was polished to a mirror with a 0.05 μm Al_2O_3 power slurry, then cleaned by sonication in deionized water, ethanol, and acetone for 3 min. GCE was then dried at room temperature. A total of 0.25 mg ordered mesoporous carbon was dispersed in 1 mL methanol solution by sonication to obtain OMC methanol solution. And 3 μL OMC methanol solution was dropped on the GCE surface. Then, 3 μL Au@ZIF-8 methanol solution (2 mg mL^{-1}) was cast on the modified GCE surface and allowed to dry at room temperature. Afterwards, 10 μL anti-CEA antibodies was immobilized onto the modified GCE surface for at least 12 h at 4 °C. Unbound antibodies were washed away with 0.01 M PBS. Electrodes were incubated in 1% BSA for 1 h to block the remaining active sites and then washed by PBS. Three microliters of various CEA concentrations was dropped on the modified electrode and incubated at 37 °C for 40 min. After being washed by PBS to remove unbound antigen, the electrodes were introduced into an electrochemical test cell and measured by DPV. The calibration plot was obtained by plotting current responses of different CEA concentrations versus the corresponding CEA concentrations. The fabrication scheme of an immunosensor is shown in Fig. 1.

Real sample determination

Blood samples of various human subjects were obtained from Shanghai Pudong Hospital. To collect a serum sample, the blood sample was centrifuged at 4000 rpm for 15 min to remove some proteins and the clear supernatant was collected for further use. Serum samples were stored at 4 °C before analysis. To determine CEA concentrations in the serum sample, serum samples (6 μL) were incubated with anti-CEA antibodies at 37 °C for 30 min. Unbound CEA was washed away with 0.01 M PBS. Then, DPV was performed in 0.1 M PBS that contained 5 mM $Fe(CN)_6^{3-/4-}$ and 0.1 M KCl from 0 to 0.6 V to record current signals of real samples. The current signals were compared with the working curve to calculate CEA concentrations in serum.

Results and discussion

Choice of materials

To obtain excellent immunosensor performance, ZIF-8 was selected for antibody immobilizing. The unique sodalite structure of ZIF-8 can provide a large specific surface area to increase antibody loading. Au NPs were attached on ZIF-8 to ensure antibodies were being anchored on ZIF-8 surface through Au-N bonds. Au NPs can also promote electron transfer and improve the biocompatibility of biosensors. OMC was used to improve electrochemical signals and increase the effective surface area of GCE due to its excellent electrical conductivity and high specific surface area.

Material characterization

The morphologies and compositions of ZIF-8 and Au@ZIF-8 were observed via various techniques. TEM images of ZIF-8 (Fig. 2a) and Au@ZIF-8 (Fig. 2b) display that the pristine ZIF-8 crystals have a uniform hexagonal morphology with a particle size of about 200 nm. Compared with ZIF-8, the decoration of Au NPs on ZIF-8 nanoparticles did not change the shapes of ZIF-8 crystals significantly. Au NPs are uniformly dispersed on ZIF-8 without obvious agglomeration. SEM images of ZIF-8 (Fig. 2c) and Au@ZIF-8 (Fig. 2d) also suggest that the presence of Au did not affect the morphology and size of ZIF-8. FTIR spectrum and Raman spectroscopy of ZIF-8, SEM image of OMC, and elemental mapping images of Au@ZIF-8 are described in detail in the Electronic Supporting Material (ESM) (Fig. S1, Fig. S2 and Fig. S3).

TEM and SEM observations were further validated by XRD. In Fig. 3a, the diffraction spectrum of ZIF-8 is completely consistent with the simulation. No diffraction peaks from impurities are observed in the XRD patterns. The unchanged XRD patterns between ZIF-8 and Au@ZIF-

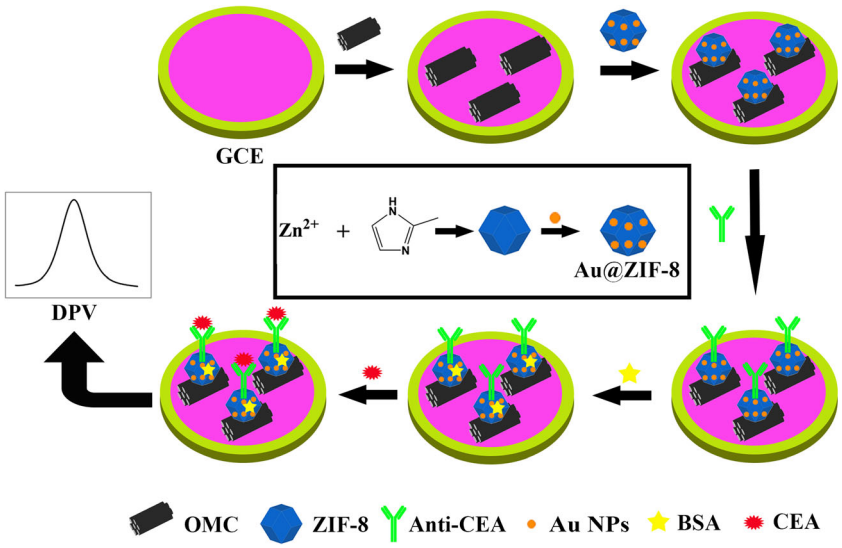

Fig. 1 Schematic illustration of fabrication of the immunosensor for CEA determination

8 nanoparticles reveal that the crystal structure of ZIF-8 nanoparticles was unaffected by Au NP decoration. In accordance with the analysis of the TEM and SEM results mentioned above, the XPS spectra of Au/ZIF-8 further confirm the existence of Au NPs on the surface of ZIF-8. XPS spectra show that Au 4f 7/2 and Au 4f 5/2 appear at 84.1 eV and 87.6 eV, respectively (Fig. 3c). This means that the Au element exists in zero valence [25]. Figure 3 d is an XPS diagram of the Zn element with two binding energies at 1021.8 eV and 1044.8 eV, which correspond to Zn2p 3/2 and Zn2p 1/2, respectively [26, 27]. The binding energy of N 1s is about 399 eV (Fig. 3e), which is assigned to C–N bonds existing in a 5-membered imidazole ring [28].

Characteristics of different electrodes

The electron transfer kinetics for the Au NPs@ZIF-8/OMC/GCE along with Au NPs@ZIF-8/GCE, bare GCE, ZIF-8/GCE, anti-CEA/Au NPs@ZIF-8/OMC/GCE, and CEA/anti-CEA/Au NPs@ZIF-8/OMC/GCE were investigated using CV in 0.1 M KCl that contained 5 mM $Fe(CN)_6^{3-/4-}$ at a scan rate of 50 mV s^{-1}. In Fig. 4a, the peak current intensity of Au NPs@ZIF-8/OMC/GCE is larger than that of Au NPs@ZIF-8/GCE. This indicates that OMC enhanced the electrochemical performance of GCE significantly. The peak current obviously decreased after ZIF-8 was dropped on an electrode. This was ascribed to the nonconducting properties of ZIF-8.

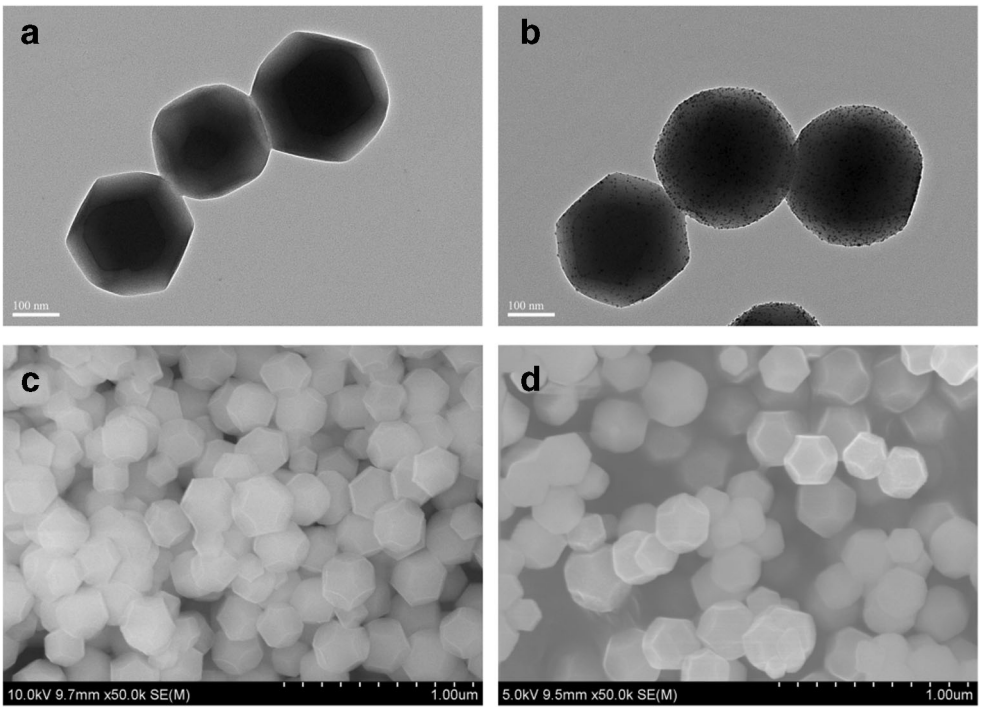

Fig. 2 **a** TEM image of ZIF-8; **b** TEM image of Au@ZIF-8; **c** SEM image of ZIF-8; **d** SEM image of Au@ZIF-8

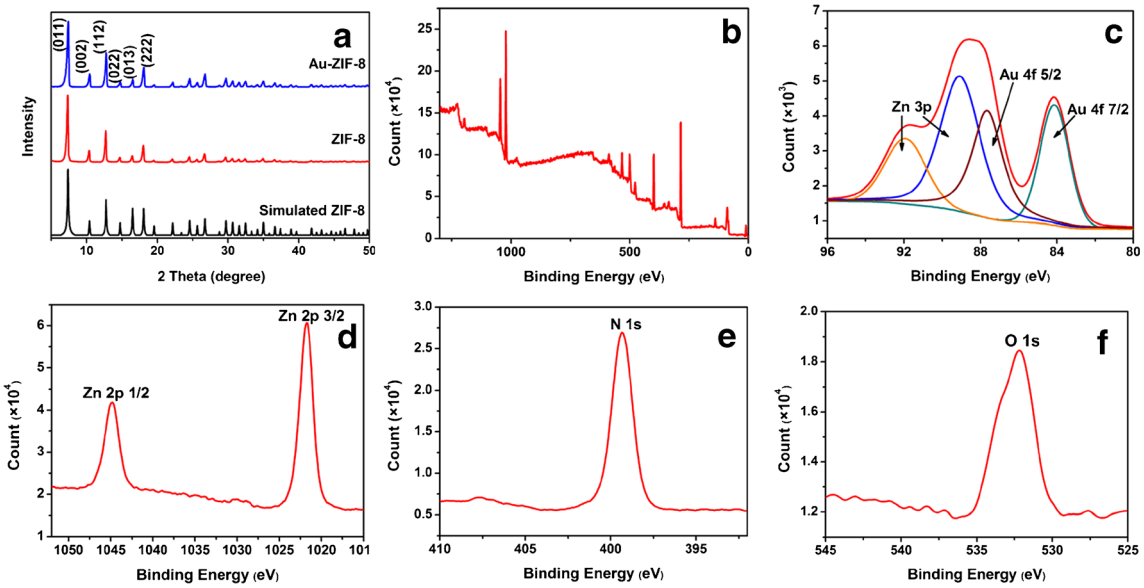

Fig. 3 **a** XRD patterns of Au@ZIF-8, ZIF-8, and situated ZIF-8; **b** XPS survey spectra of Au@ZIF-8; **c** Au 4f spectrum; **d** Zn 2p spectrum; **e** N 1s spectrum; **f** O 1s spectrum

Compared with ZIF-8/GCE, an increase in the redox peak current for Au NPs@ZIF-8/GCE was observed due to the good conductivity of Au NPs. After anti-CEA was deposited on Au NPs@ZIF-8/OMC modified electrode, a significant decrease in peak current intensity was clearly observed. This suggests that the anti-CEA layer was successfully immobilized on the surface of a modified electrode. Critical reduction of peak current is observed upon binding CEA to anti-CEA antibody. This is attributed to the formation of an immunocomplex layer by CEA and anti-CEA combination. The cyclic voltammogram of Au NPs@ZIF-8/OMC/GCE modified GCE represents quasi-reversible redox peak currents at 0.307 (E_{pa}) and 0.234 V (E_{pc}). The peak-to-peak separation is found to be around 73 mV and the ratio of the anodic to cathodic peak currents almost close to unity 1.

ElS spectra of electrodes before and after each step of modifications are shown in Fig. 4b. Au@ZIF-8 modified GCE presented smaller electron transfer resistance than ZIF-8

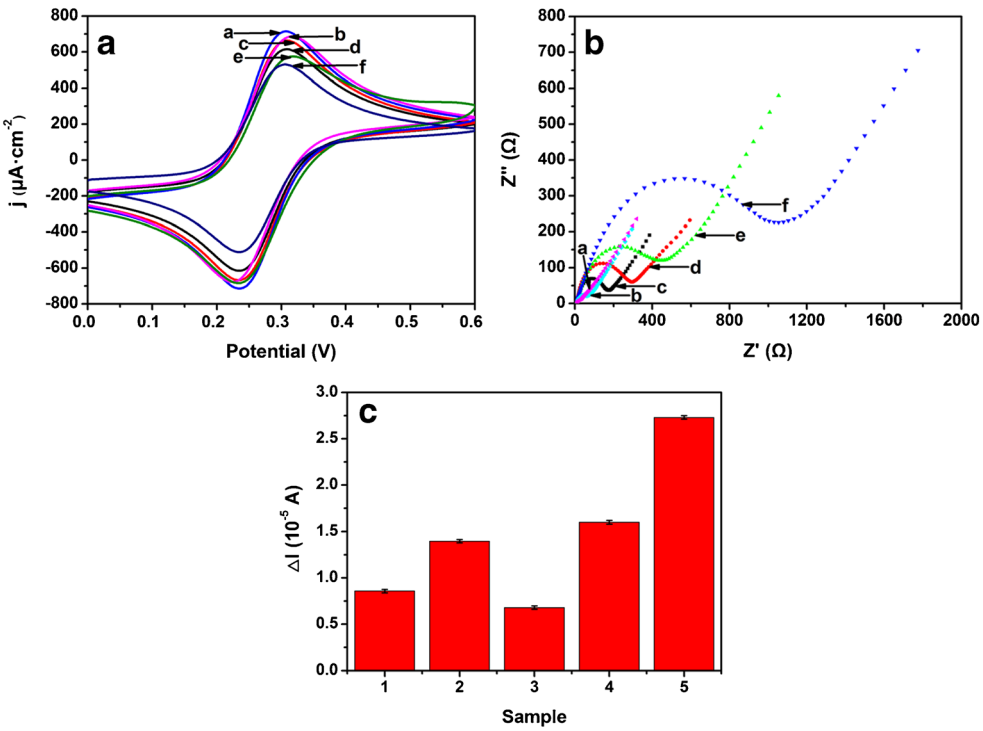

Fig. 4 **a** Cyclic voltammetry curves of Au@ZIF-8/OMC/GCE (curve a), bare GCE (curve b), Au@ZIF-8/GCE (curve c), ZIF-8/GCE (curve d), anti-CEA/Au@ZIF-8/OMC/GCE (curve e), CEA/anti-CEA/Au@ZIF-8/OMC/GCE (curve f); **b** EIS of Au@ZIF-8/OMC/GCE (curve a), bare GCE (curve b), Au@ZIF-8/GCE (curve c), ZIF-8/GCE (curve d), anti-CEA/Au@ZIF-8/OMC/GCE (curve e), CEA/anti-CEA/Au@ZIF-8/OMC/GCE (curve f); **c** DPV current change (ΔI_{DPV}) determine 100 ng mL^{-1} CEA using electrodes modified by ZIF-8 (1), Au@ZIF-8 (2), OMC (3), ZIF-8/OMC (4), Au@ZIF-8/OMC (5) in 0.1 M KCl that contained 5 mM $[Fe(CN)_6]^{3-/4-}$ ($n = 3$)

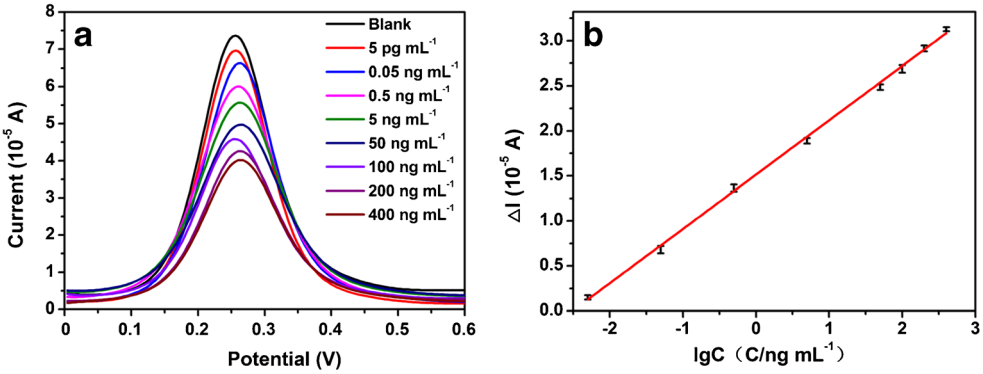

Fig. 5 **a** DPV response curves of the immunosensor toward different concentrations of CEA (0.005, 0.05, 0.5, 5, 50, 100, 200, 400 ng mL^{-1}) under optimal conditions. **b** The responding calibration plot ($n = 3$)

modified GCE. Due to the slow electron transfer kinetics of proteins, immobilization of antibody on modified electrode and combination between CEA and anti-CEA antibody lead to the increase of electron transfer resistance. This is in agreement with CV results. To further indicate the enhanced electrochemical sensing performance of Au NPs@ZIF-8/OMC, different types of modified electrodes were measured in the existence of 100 ng mL^{-1} CEA using DPV (Fig. 4c). The results show that the change of DPV peak current (ΔI_{DPV}) from Au NPs@ZIF-8 is significantly higher than that of ZIF-8, and the peak current change value of Au NPs@ZIF-8/OMC is higher than that of Au NPs@ZIF-8 modified electrode. This is because the presence of Au NPs provides a large number of binding sites for antibody and the appearance of OMC promotes electronic transfer, thus improving electrochemical responses.

Optimization of experimental conditions

The following parameters were optimized: (a) concentration ratio of Au@ZIF-8 to OMC; (b) concentration of anti-CEA; (c) reaction time; (d) incubation temperature; (e) sample pH value. Respective text and figures on optimizations are given in the Electronic Supporting Material. In short, the following experimental conditions were found to give the best results: (a) optimal concentration ratio 8:1; (b) optimal loading 20 μg mL^{-1}; (c) reaction time 30 min; (d) incubation temperature 35 °C; (e) best sample pH value 7.4.

Analytical performance of the immunosensor

The response studies of this immunosensor were investigated using DPV. DPV results of different CEA concentrations were measured under optimized conditions. Figure 5a exhibits the sensing performance of anti-CEA/Au NPs@ZIF-8/OMC/GCE for a series of different CEA concentrations ranging from 5 pg mL^{-1} to 400 ng mL^{-1}. The peak current decreases with increasing CEA concentrations, which is ascribed to the insulating layer formed by antigen antibody binding. It is found that ΔI_{DPV} is linearly related to the logarithm of CEA concentration in the analyte concentration range of 5 pg mL^{-1} to 400 ng mL^{-1} (Fig. 5b). The linear relationship between ΔI_{DPV} and logarithmic value of CEA concentration demonstrates that the current response was the direct result of antigen-antibody binding. The linear regression equation is $\Delta I = 0.6032 \log(C_{CEA}) + 1.5053$ with correlation coefficient of 0.9986 and low limit of determination (LOD) of 1.3 pg mL^{-1} ($S/N = 3$). The sensitivity is calculated as 37.96 μA·log(ng mL^{-1})·cm^{-2}. Generally, the CEA level in healthy people is less than 5 ng mL^{-1}. The average CEA concentration of 5.0 ng mL^{-1} in human serum is considered a cutoff value to distinguish abnormal from normal levels.

Table 1 Comparison of different methods for CEA determination

Method applied	Material	Linear range (ng mL^{-1})	LOD (pg mL^{-1})	Reference
Fluorescence	ZIF-8/CD/TP	0.01–5	10	[29]
Photoelectrochemistry	ZIF-8-Assisted NaYF4:Yb,Tm@ZnO	0.1–300	32	[30]
Differential pulse voltammetry	Au@OMC	0.05–20	13	[31]
Electrochemical impedance spectroscopy	Au/FU-NCNT	0.01–10	6.84	[32]
Cyclic voltammetry	Ag NPs-rGO	50–500	35,000	[33]
Electrochemical impedance spectroscopy	Graphene	1–25	230	[34]
Electroluminescence	GO/MWCNTs-COOH/Au@CeO_2	0.05-100	20	[35]
Differential pulse voltammetry	Au NPs@ZIF-8/OMC	0.005–400	1.33	This work

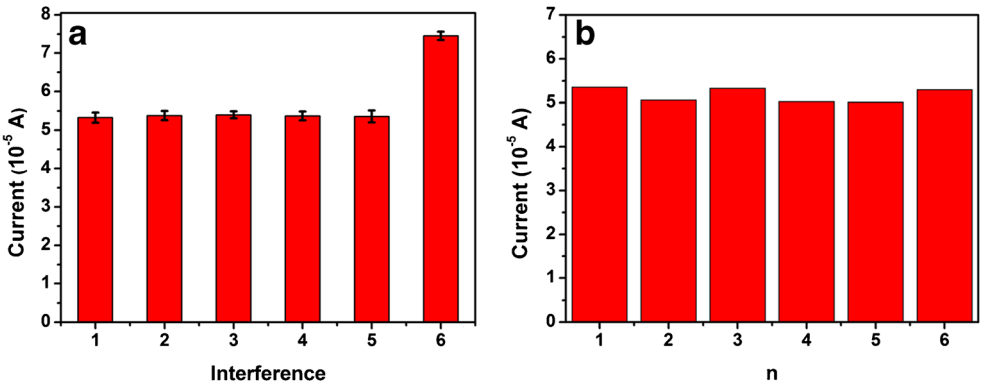

Fig. 6 **a** Specificity of this immunoassay for 10 ng mL^{-1} CEA + 100 ng mL^{-1} AFP (1), 10 ng mL^{-1} CEA + 1 μg mL^{-1} HCG (2), 10 ng mL^{-1} CEA + 100 ng mL^{-1} BSA (3), 10 ng mL^{-1} CEA + 100 ng mL^{-1} IgG (4), 10 ng mL^{-1} CEA (5), interference without CEA (6) ($n = 3$). **b** Current response of six different electrodes treated in the same way for reproducibility study

Therefore, this immunosensor can completely meet the needs of clinical diagnosis toward CEA.

In order to further demonstrate the superior performance of this immunosensor, the analytical performance of this method is compared with that of previously reported methods (Table 1). According to this comparison, the determination limit of this method is lower than that of the method reported previously. The linear range of this method is much wider than most of the immunosensors. The excellent performance of this sensor can be attributed to the combination of Au@ZIF-8 and OMC. Firstly, the large surface area of ZIF-8 can effectively increase antibody immobilization. Secondly, OMC can enhance the conductivity of biosensor by high electron transfer ability. Although a limitation of this technology is that it is a single-analyte assay, this biosensor exhibits unique advantages including rapid response, straightforward fabrication, and use of lesser chemicals and reagents. These advantages make it highly suitable for personalized POCT (point-of-care testing) and decentralization of healthcare management. Compared with other methods, this proposed sensor is expected to build small instruments to realize POCT in future.

Specificity, stability, and reproducibility and regeneration of this immunosensor

The selectivity of this immunosensor was studied through comparing the electrochemical responses of 10 ng mL^{-1} CEA with and without interference. Some proteins in human plasma including 1 μg mL^{-1} HCG, 100 ng mL^{-1} AFP, 100 ng mL^{-1} IgG, and 100 ng mL^{-1} BSA were applied as typical interfering species [36–38]. As shown in Fig. 6a, DPV current responses with and without interferents show insignificant variations. This clearly demonstrates that no interaction occurred between the antibodies and interfering species. Thus, this immunosensor has high specificity. To investigate the stability of the immunosensor, electrodes were modified in the same procedure and stored in the PBS at 4 °C. Current responses were recorded by DPV measurements. As shown in Table S1, the current responses of the immunosensor remained 96% after 1 week, 94.8% of the initial response after 10 days. This suggests that the activity of anti-CEA antibody was effectively maintained and the stability of such sensor was also satisfactory. Reproducibility of the immunosensor was further analyzed by preparing a set of modified electrodes independently fabricated within the same batch for determining 5 ng mL^{-1} CEA. In Fig. 6b, the relative standard deviation (RSD) of 3.2% from all of the six electrodes indicates acceptable reproducibility of this immunosensor.

Real sample analysis

To evaluate the feasibility of this immunosensor in real biological samples, a recovery test with different CEA concentrations in diluted serum samples was carried out. The conditions of the antigen-antibody interaction are consistent with the previous experiments. Several human serum samples diluted 100-fold by PBS to minimize nonspecific adsorption were analyzed in the presence of 10, 50, and 100 ng mL^{-1} CEA. In Table 2, the recovery is found to be in the range of 101–103% and the corresponding RSD is in the range of 4.15–8.29%, respectively. In addition, CEA concentrations of 4 clinical serum samples were detected using this method and

Table 2 Determination of CEA in real samples ($n = 3$)

No.	Added (ng mL^{-1})	Total found (mean ± SD%, ng mL^{-1}, $n = 3$)	Recovery (%)	RSD (%)
1	10	10.13 ± 0.84	101	8.29
2	50	52.5 ± 1.46	105	2.78
3	100	103 ± 4.27	103	4.15

the results are compared with reference data from a Siemens Advia Centaur XP chemiluminescence immunoassay analyzer. In Table S2, the relative error between two methods was in the range of 2.82–5.31%. These acceptable results indicated that this immunosensor had significant potential for determination of CEA in clinical diagnostics.

Conclusion

In this work, an electrochemical immunoassay for CEA determination was constructed by using Au NPs modified ZIF-8 and OMC. Au NPs@ZIF-8 nanoparticles with a large surface area were used to increase antibody loading. OMC can enhance the conductivity of biosensors due to high electron transfer ability. The synergistic effect between Au NPs@ZIF-8 and OMC can amplify an electrochemical response effectively. This biosensor exhibited wide linear range, low determination limit, high specificity, satisfactory stability, and acceptable reproducibility. In addition, the results collected from this method were in acceptable agreement with data determined by the commercial chemiluminescence immunoassay analyzer. Future work should focus on the simultaneous determination of multiple analytes in serum.

Funding information This research was supported by the National Natural Science Fund of China (grants 81973097, 81773480, 81573200, 81673229, 81703269), Major weak subjects in Pudong New area (grants PWZbr2017-02), Shanghai Pudong Hospital Talent Project (PX201604), Natural Science Foundation of Heilongjiang Province (QC2018120), University Nursing Program for Young Scholars with Creative Talents in Heilongjiang Province (UNPYSCT-2017173), the Fundamental Research Funds for the Universities of Heilongjiang Province (2017-KYYWF-0648), and the Administration of Science & Technology Foundation of Mudanjiang (No. Z2016s0072)

Compliance with ethical standards

Ethical approval for this study has been granted by the institutional research Ethics Community of Shanghai Pudong Hospital.

Conflict of interest The authors declare that there is no conflict of interest.

References

1. Thomas DS, Fourkala EO, Apostolidou S, Gunu R, Ryan A, Jacobs I, Menon U, Alderton W, Gentry-Maharaj A, Timms JF (2015) Evaluation of serum CEA, CYFRA21-1 and CA125 for the early determination of colorectal cancer using longitudinal preclinical samples. Br J Cancer 113(2):268–274
2. Molina R, Marrades RM, Augé JM, Escudero JM, Viñolas N, Reguart N, Ramirez J, Filella X, Molins L, Agustí A (2016) Assessment of a combined panel of six serum tumor markers for lung cancer. Am J Respir Crit Care Med 193(4):427–437
3. Wu SG, He ZY, Ren HY, Yang LC, Sun JY, Li FY, Guo L, Lin HX (2016) Use of CEA and CA15-3 to predict axillary lymph node metastasis in patients with breast cancer. J Cancer 7(1):37–41
4. Liu L, Xu H, Wang W, Wu C, Chen Y, Yang J, Cen P, Xu J, Liu C, Long J, Guha S, Fu D, Ni Q, Jatoi A, Chari S, McCleary-Wheeler AL, Fernandez-Zapico ME, Li M, Yu X (2015) A preoperative serum signature of CEA+/CA125+/CA19-9 ≥ 1000 U/mL indicates poor outcome to pancreatectomy for pancreatic cancer. Int J Cancer 136(9):2216–2227
5. Honma M, Iinuma S, Kanno K, Komatsu S, Minami-Hori M, Iizuka H, Ishida-Yamamoto A (2016) Serum carcinoembryonic antigen (CEA) as a clinical marker in acquired idiopathic generalized anhidrosis: a close correlation between serum CEA level and disease activity. J Eur Acad Dermatol Venereol 30(8):1379–1383
6. Liu J, Shang Y, Zhu Q, Zhang X, Zheng J (2019) A voltammetric immunoassay for the carcinoembryonic antigen using silver(I)-terephthalate metal-organic frameworks containing gold nanoparticles as a signal probe. Mikrochim Acta 186:509
7. Xu L, Liu Z, Lei S, Huang D, Zou L, Ye B (2019) A sandwich-type electrochemical aptasensor for the carcinoembryonic antigen via biocatalytic precipitation amplification and by using gold nanoparticle composites. Mikrochim Acta 186:473
8. Zhang B, Jia Y, Wang J, Hu X, Zhao Z, Cheng Y (2019) Cysteine-assisted photoelectrochemical immunoassay for the carcinoembryonic antigen by using an ITO electrode modified with C3N4-BiOCl semiconductor and CuO nanoparticles as antibody labels. Mikrochim Acta 186:633
9. Zheng X, Li L, Cui K, Zhang Y, Zhang L, Ge S, Yu J (2018) Ultrasensitive enzyme-free biosensor by coupling cyclodextrin functionalized au nanoparticles and high-performance Au-paper electrode. ACS Appl Mater Interfaces 10(4):3333–3340
10. Chen Y, Chu W, Liu W, Guo X, Jin Y, Li B (2018) Paper-based chemiluminescence immunodevice for the carcinoembryonic antigen by employing multi-enzyme carbon nanosphere signal enhancement. Microchim Acta 185(3):187
11. Pal S, Bhand S (2015) Zinc oxide nanoparticle-enhanced ultrasensitive chemiluminescence immunoassay for the carcinoma embryonic antigen. Microchim Acta 182(9–10):1643–1651
12. Grasso L, Wyss R, Weidenauer L, Thampi A, Demurtas D, Prudent M, Lion N, Vogel H (2015) Molecular screening of cancer-derived exosomes by surface plasmon resonance spectroscopy. Anal Bioanal Chem 407(18):5425–5432
13. Shekari Z, Zare HR, Falahati A (2019) Electrochemical sandwich aptasensor for the carcinoembryonic antigen using graphene quantum dots, gold nanoparticles and nitrogen doped graphene modified electrode and exploiting the peroxidase-mimicking activity of a G-quadruplex DNAzyme. Mikrochim Acta 186:530
14. Tan Z, Cao L, Yang Y, Yan Q, Liu Q, Zhang W, Zhao P, Li Y, Zhang D (2019) Amperometric immunoassay for the carcinoembryonic antigen by using a peroxidase mimic consisting of palladium nanospheres functionalized with glutathione-capped gold nanoparticles on graphene oxide. Mikrochim Acta 186:693
15. Gan T, Li J, Li H, Liu Y, Xu Z (2019) Synthesis of Au nanorod-embedded and graphene oxide-wrapped microporous ZIF-8 with high electrocatalytic activity for the sensing of pesticides. Nanoscale
16. Pimentel BR, Lively RP (2018) Propylene enrichment via kinetic vacuum pressure swing adsorption using ZIF-8 fiber sorbents. ACS Appl Mater Interfaces 10(42):36323–36331
17. Su L, Wu Q, Tan L, Huang Z, Fu C, Ren X, Xia N, Chen Z, Ma X, Lan X, Zhang Q, Meng X (2019) High biocompatible ZIF-8 coated by ZrO for chemo-microwave thermal tumor synergistic therapy. ACS Appl Mater Interfaces 11(11):10520–10531
18. Dong S, Tong M, Zhang D, Huang T (2017) The strategy of nitrite and immunoassay human IgG biosensors based on ZnO@ZIF-8

and ionic liquid composite film. Sensors Actuators B Chem 251: 650–657
19. Wang H, Ma Z (2019) "Off-on" signal amplification strategy amperometric immunosensor for ultrasensitive detection of tumour marker. Biosens Bioelectron 132:265–270
20. Ladmakhi HB, Chekin F, Fathi S, Raoof JB (2020) Electrochemical sensor based on magnetite graphene oxide/ordered mesoporous carbon hybrid to detection of allopurinol in clinical samples. Talanta 211:120759
21. Liu C, Pei W-Y, Li J-F, Yang J, Ma J-F (2020) Calix[4]arene-based [Co4] complex/ordered mesoporous carbon as a high-performance electrocatalyst for efficient detection of baicalein. Sensors Actuators B Chem 308:127677
22. Regiart M, Fernandez-Baldo MA, Villarroel-Rocha J, Messina GA, Bertolino FA, Sapag K, Timperman AT, Raba J (2017) Microfluidic immunosensor based on mesoporous silica platform and CMK-3/poly-acrylamide-co-methacrylate of dihydrolipoic acid modified gold electrode for cancer biomarker detection. Anal Chim Acta 963:83–92
23. Yang L, Zhao H, Deng G, Ran X, Li Y, Xie X, Li C-P (2015) Immunosensor for prostate-specific antigen using Au/Pd@flower-like SnO2 as platform and Au@mesoporous carbon as signal amplification. RSC Adv 5:74046–74053
24. Wang Z, Wang Z, Lin S, Jin H, Gao S, Zhu Y, Jin J (2018) Nanoparticle-templated nanofiltration membranes for ultrahigh performance desalination. Nat Commun 9(1):2004
25. Cuenya BR, Baeck SH, Jaramillo TF, McFarland EW (2003) Size- and support-dependent electronic and catalytic properties of Au0/Au3+ nanoparticles synthesized from block copolymer micelles. J Am Chem Soc 125(42):12928–12934
26. Tian F, Cerro AM, Mosier AM, Wayment-Steele HK, Shine RS, Park A, Webster ER, Johnson LE, Johal MS, Benz L (2014) Surface and stability characterization of a nanoporous ZIF-8 thin film. J Phys Chem C 118(26):14449–14456
27. Zhang Y, Xie Z, Wang Z, Feng X, Wang Y, Wu A (2016) Unveiling the adsorption mechanism of zeolitic imidazolate framework-8 with high efficiency for removal of copper ions from aqueous solutions. Dalton Trans 45(32):12653–12660
28. Li N, Zhou L, Jin X, Owens G, Chen Z (2019) Simultaneous removal of tetracycline and oxytetracycline antibiotics from wastewater using a ZIF-8 metal organic-framework. J Hazard Mater 366: 563–572
29. Yan H, Jiao L, Wang H, Xu W, Wu Y, Gu W, Du D, Lin Y, Zhu C (2019) A "sense-and-treat" ELISA using zeolitic imidazolate framework-8 as carriers for dual-modal detection of carcinoembryonic antigen. Sensors Actuators B Chem 297:126760
30. Lv S, Zhang K, Zhu L, Tang D (2020) ZIF-8-assisted NaYF4:Yb, Tm@ZnO converter with exonuclease III-powered DNA walker for near-infrared light responsive biosensor. Anal Chem 92:1470–1476
31. Wu D, Guo A, Guo Z, Xie L, Wei Q, Du B (2014) Simultaneous electrochemical detection of cervical cancer markers using reduced graphene oxide-tetraethylene pentamine as electrode materials and distinguishable redox probes as labels. Biosens Bioelectron 54: 634–639
32. Meng Y, Song Y, Guo C, Cui B, Ji H, Ma Z (2019) Tailoring the dimensionality of carbon nanostructures as highly electrochemical supports for detection of carcinoembryonic antigens. RSC Adv 9: 13431–13443
33. Lee SX, Lim HN, Ibrahim I, Jamil A, Pandikumar A, Huang NM (2017) Horseradish peroxidase-labeled silver/reduced graphene oxide thin film-modified screen-printed electrode for detection of carcinoembryonic antigen. Biosens Bioelectron 89(Pt 1):673–680
34. Singh VK, Kumar S, Pandey SK, Srivastava S, Mishra M, Gupta G, Malhotra BD, Tiwari RS, Srivastava A (2018) Fabrication of sensitive bioelectrode based on atomically thin CVD grown graphene for cancer biomarker detection. Biosens Bioelectron 105:173–181
35. Pang X, Li J, Zhao Y, Wu D, Zhang Y, Du B, Ma H, Wei Q (2015) Label-free electrochemiluminescent immunosensor for detection of carcinoembryonic antigen based on nanocomposites of GO/MWCNTs-COOH/Au@CeO_2. ACS Appl Mater Interfaces 7: 19260–19267
36. Jiang W, Liu L, Zhang L, Guo Q, Cui Y, Yang M (2017) Sensitive immunosensing of the carcinoembryonic antigen utilizing aptamer-based in-situ formation of a redox-active heteropolyacid and rolling circle amplification. Microchim Acta 184(12):4757–4763
37. Lv P, Min L, Yuan R, Chai Y, Chen S (2010) A novel immunosensor for carcinoembryonic antigen based on poly(diallyldimethylammonium chloride) protected prussian blue nanoparticles and double-layer nanometer-sized gold particles. Microchim Acta 171(3–4):297–304
38. Si Z, Xie B, Chen Z, Tang C, Li T, Yang M (2017) Electrochemical aptasensor for the cancer biomarker CEA based on aptamer induced current due to formation of molybdophosphate. Microchim Acta 184(9):3215–3221